JOURNAL OF GEOPHYSICAL RESEARCH, VOL. 105, NO. B2, PAGES 3135–3149, FEBRUARY 10, 2000

Syntectonic melt pathways during simple shearing of a partially molten rock analogue (Norcamphor-Benzamide)

Claudio L. Rosenberg and Mark R. Handy

Institut für Geowissenschaften, Justus-Liebig Universität, Giessen, Germany

Abstract. Norcamphor-benzamide aggregates were used as analogues for partially molten quartzofeldspathic rock. Drained, constant displacement rate, simple shearing of partially molten norcamphor-benzamide aggregates produces strain localization within melt-bearing, extensional shear fractures. These fractures interconnect to form shear surfaces whose orientation with respect to the shear zone boundary is like that of synthetic shear bands (C' surfaces) in naturally deformed, mylonitic rocks. The shear bands channel overpressured melt from dilatant grain boundaries in the norcamphor-benzamide aggregate to undeformed, low-pressure areas adjacent to the deforming sample. The rapid expulsion of melt in the aggregate along shear bands hinders the attainment of a rheological critical melt percentage (20%) within the shear zone as a whole. However, this melt percentage is achieved within the melt-bearing shear bands. Deformation within the shear bands involves a strain-dependent switch from intergranular fracturing and dislocation creep to diffusion-accommodated, grain-boundary sliding, whereas the matrix adjacent to the shear bands continues to deform by dislocation creep. At a shear strain of approximately $\gamma = 0.7$ the melt-bearing shear bands coalesce to form interconnected weak layers subparallel to the shear zone boundaries. The strength of the aggregate could not be measured but is inferred to decrease markedly once the melt-bearing layers interconnect. When the melt completely crystallizes and deformation ceases, the former presence of melt within the shear bands is only betrayed by the alignment of benzamide grain boundaries parallel to the shear bands.

1. Introduction

Understanding how melt segregates during deformation is of fundamental importance for refining rheological models of the lithosphere in tectonic settings as diverse as mid-ocean ridges and the roots of orogens. Granitic melt occupies many structurally controlled sites [e.g., *Collins and Sawyer*, 1996], particularly shear zones [e.g., *Hutton*, 1982; *Hollister and Crawford*, 1986; *Davidson et al.*, 1992; *Brown*, 1994] and shear bands [*Sawyer*, 1991; *Rey et al.*, 1992; *Vauchez and Egydio da Silva*, 1992; *Hartel and Pattison*, 1996]. Yet little is known about how granitic melt is distributed on the granular scale during deformation. Although the former presence of melt on this scale can be inferred from metamorphic mineral assemblages [e.g., *Hartel and Pattison*, 1996], the actual melt pathways usually have been obliterated by slow crystallization and dynamic or static recrystallization. Examples of naturally deformed rock with relict, syntectonic grain-scale melt topology are accordingly rare [*Cesare et al.*, 1997; *Sawyer*, 1999; *Rosenberg and Riller*, 2000]. Therefore current understanding of deformation mechanisms and melt segregation and accumulation processes in anatectic rock relies primarily on theoretical [e.g., *Stevenson*, 1989] and experimental work (see *Rutter* [1997] for a review of granites and *Kohlstedt and Zimmerman* [1996] for a review of mantle rocks).

Unfortunately, experimental deformation of partially molten granitic rocks generally fails to reproduce microstructures observed in naturally deformed, anatectic granites [*Rosenberg and Riller*, 2000]. This is because the low viscosities and high strain rates required to maintain reasonable experimental times (hours to days) can only be attained at experimental temperatures well exceeding those in nature. At these experimental temperatures, granites produce larger melt fractions than do natural rocks with comparable volume proportions of constituent solid phases. High experimental strain rates, particularly in the presence of a melt, favor embrittlement at temperatures that in naturally deforming rocks only involve dislocation creep and/or melt-assisted diffusional creep. Another problem is that previous experiments were undrained; that is, the melt was constrained to remain within the sample throughout deformation. Undrained experiments obviously preclude melt segregation at the sample scale, whereas melt accumulations that have segregated from deforming, partially molten protoliths are commonly observed both in mantle rocks [e.g., *Nicolas*, 1986] and migmatites [e.g., Collins and Sawyer, 1996].

Another experimental method is to deform rock-analogue materials in a shear box at room temperature and pressure, utilizing two solid phases with a very large viscosity contrast (e.g., 300:1 by *Grujic and Mancktelow* [1998]), such that the weaker phase simulates melt in a rock. Such experiments are useful for studying strain partitioning between melt and solid rock at constant volume proportions of melt [*Grujic and Mancktelow*, 1998] or the development of shape preferred orientations during magmatic flow [*Ildefonse and Mancktelow*, 1993; *Ildefonse et al.*, 1997; *Arbaret et al.*, 1996]. However, the two phases cannot react with each other as a natural melt does with its host rock. Therefore important syntectonic processes such as crystallization, melting, and changes in grain shape and size cannot be simulated.

Copyright 2000 by the American Geophysical Union

Paper number 1999JB900371
0148-0227/00/1999JB900371$09.00

Deformation experiments on rock analogue materials performed under an optical microscope allow one to observe and record microstructural changes throughout the deformational history [*Means*, 1977, 1989]. Using this "in-situ" or "see-through" approach, *Park and Means* [1996] successfully investigated microstructural changes in a crystal-melt mixture containing three solid phases (ammonium thiocyanate, ammonium chloride, and diammonia tetrathiocyanato cobaltate) that crystallized from a eutectic melt. This work clearly demonstrates the importance of interactions between melt and solid and shows that crystals do not necessarily behave as rigid particles within the melt matrix.

In this paper, we report on a series of drained, see-through deformation experiments on partially molten, norcamphor-benzamide aggregates. This binary-eutectic system is very weak at the laboratory conditions of deformation, and its behavior is predominantly viscous, even at very large grain sizes (up to 1 mm) and in the presence of a melt. It is therefore ideally suited for studying syntectonic melt segregation in rocks on the grain and thin section scales. Following a description of the experimental materials and conditions in section 2, we describe the melt topology during melting under hydrostatic conditions and briefly outline the solid-state microstructures that develop in melt-free deformation experiments. The behavior of the melt and solid phases under these reference conditions is important for interpreting the more complicated melt topologies and microstructures in the deformational experiments on partially molten aggregates. We found that extensional shear surfaces developed on the granular and supragranular scales serve as conduits for the migration of pressurized melt through the aggregate. In section 6 we discuss the results of our experiments in the context of several questions posed by previous studies of partially molten rocks and rock analogues. We conclude by assessing the kinematic and dynamic roles of localized shearing during anatexis.

2. Experimental Materials and Conditions

The experiments involve shearing a thin wafer of organic compound between two glass plates (thin section plates) in a modified Means-Urai deformation rig [e.g., *Means* 1989, *Bauer et al.*, 2000], as depicted in Figure 1. Each glass plate has an etched or "frosted" strip which grips the organic material and thus transfers the displacement of the piston to the sample via the upper plate. The frosted grips therefore define the shear zone boundaries (Figure 1c). We conducted simple shear experiments at constant shear strain rates of $\gamma = 6.94 \times 10^{-5}\ s^{-1}$ and $8.68 \times 10^{-5}\ s^{-1}$ (for 2.5 and 2 mm spacing, respectively, between the frosted grips) at the constant displacement rate of the driving motor.

For the purposes of this study we concocted a two-phase aggregate of 90-95 wt % norcamphor ($C_7H_{10}O$, probably hexagonal: Bons, 1993) and 5-10 wt % benzamide ($C_6H_5CONH_2$, monoclinic). The melting temperature of benzamide is 132°C, whereas that of norcamphor is 96-98°C. The eutectic temperature of the norcamphor-benzamide aggregate is 42°C. The eutectic composition is characterised by ~ 20 wt % benzamide and 80 wt % norcamphor. However, chemical equilibrium was not attained in the present experiments.

Although we did not systematically measure melt-norcamphor dihedral angles, we observed that melt-norcamphor-norcamphor dihedral angles under static conditions are small, clearly < 60°. This suggests that melt forms an interconnected network along three- and four-grain junctions [e.g., *Laporte et al.*, 1997], as observed in most synthetic silicate systems (e.g., quartz aggregtes and feldspar aggregates in contact with a granitic melt [*Laporte et al.*, 1997] or olivine aggregates in contact with a basaltic melt [*Hirth and Kohlstedt*, 1995a].

Samples are prepared so as to allow melt to drain from the deforming norcamphor-benzamide aggregate into an undeformed or less deformed part of the experimental system, while ensuring that the total volume of the system (i.e., norcamphor-benzamide aggregate, melt, and solid frames described below) does not change during deformation. Initially, norcamphor and benzamide are mixed with small amounts of fine-grained corundum (average grain size of 9 μm) grinding powder. The corundum particles do not chemically interact with norcamphor and benzamide, they do not inhibit grain boundary migration of norcamphor, and they behave as passive markers during deformation. Therefore they serve as reliable strain markers. The mixture is then cold pressed at room temperature to a thickness of 150 to 200 μm. A 1 cm x 1.5 mm tablet is cut from this pressed aggregate and positioned between the frosted grips on the thin sections (Figure 1b) so as not to touch the frosted grips. The tablet of norcamphor-benzamide is then enclosed within a frame of pure norcamphor (Figure 1b). This frame is prepared by cutting a rectangular piece from the middle of a previously cut norcamphor tablet. The norcamphor frame has two functions: First, it forms a solid barrier to melt generated within the norcamphor-benzamide aggregate between the frosted grips (i.e., shear zone boundaries). This is because the norcamphor frame melts at higher temperatures than the experimental temperature required to melt the norcamphor-benzamide aggregate. Also, its thickness generally does not exceed one grain diameter, therefore preventing the formation of a three-dimensional network of grain edges along which melt could migrate out of the sample. This allows us to interpret the occurrence of melt in the norcamphor frame during and after as the result of melt migration from the central part of the sample outwards. Second, the norcamphor frame acts as a solid medium that effectively transfers/relays the force of the moving glass plate to the soft, partially molten norcamphor-benzamide sample. As a further measure to prevent any melt from leaving the system during deformation, the norcamphor-benzamide aggregate and norcamphor frame are both enclosed in a larger frame of a viscous polymer material (Figure 1b) polydimethyl-siloxane or PDMS (see *Weijermars* [1986] for a discussion of its rheology). The sample is then annealed within the deformation apparatus at 38°C for 4 to 7 days. The mean diameters of the annealed norcamphor and benzamide grains in the undeformed aggregate were 140 μm and 50 μm, respectively.

Without the rather elaborate system of melt barriers described above, we found that randomly oriented melt channels formed across the shear zone boundaries upon melting, even in the absence of deformation. This obviously obscures any relationship between deformation and melt segregation. The associated volume loss of the unconfined,

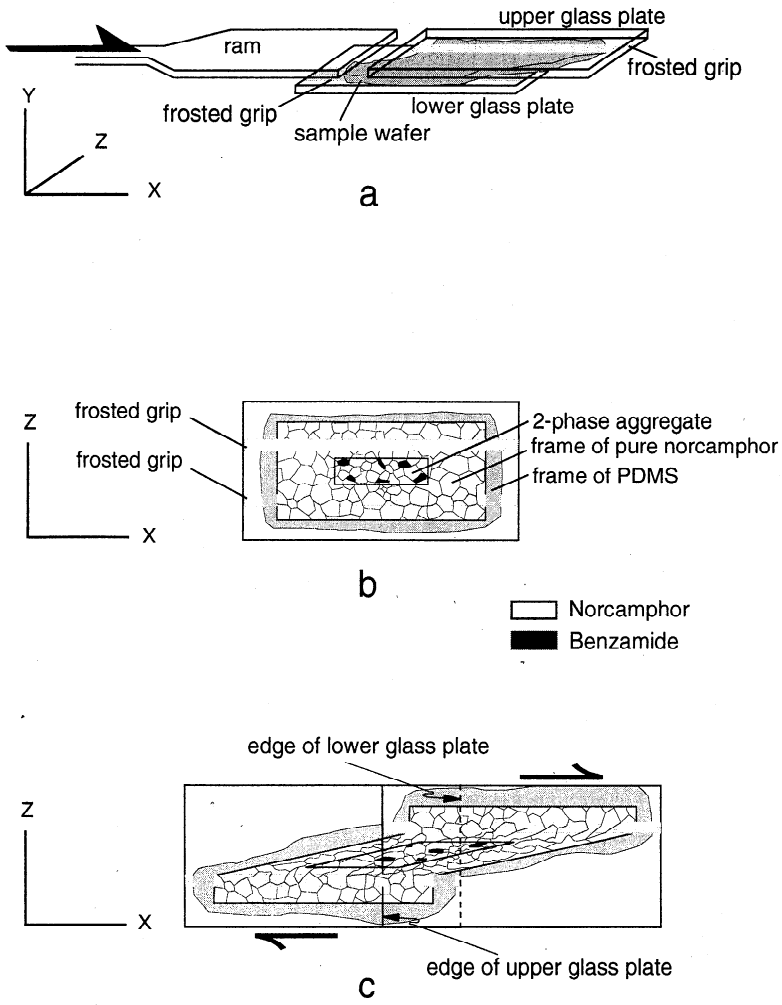

Figure 1. (a) Sample configuration used in experiments. The ram moves the upper glass plate with respect to the fixed, lower glass plate, thereby shearing the aggregate. *XYZ* are kinematic axes for simple shearing experiment. (b) View of *XZ* fabric plane before deformation. The norcamphor-benzamide aggregate is situated between the frosted grips and enclosed in a frame of norcamphor. This is, in turn, sealed within a frame of PDMS. (c) View of *XZ* fabric plane after simple shearing.

unmelted norcamphor-benzamide aggregates also precludes meaningful strain analyses within the sample shear zone. We found that strain analysis using corundum markers is possible up to a shear strain of about $\gamma = 1$ from the onset of melting. During this strain interval, melt does not escape from the shear zone. As shown below, however, melt drainage from the norcamphor-benzamide aggregates in our confined experiments is deformationally induced at higher strains.

The microstructural evolution during deformation was recorded with color slides, black and white photographs, and videotapes taken through a microscope at a maximum magnification of 64X. This low magnification possibly limited our ability to detect very small amounts of melt along some grain boundaries.

Identifying the melt during the experiments was difficult because melt is opaque under crossed polarized light, rendering it indistinguishable from crystals and crystal domains at complete optical extinction. We overcame this problem by viewing the sample in plane (unpolarized) reflected light. In reflected light the melt appears somewhat lighter than adjacent norcamphor and benzamide grains. In some cases we stopped the deformation and quenched the melt to a brown, microcrystalline aggregate that could be easily distinguished from the unmelted norcamphor and benzamide grains. The volume proportion of melt in the samples was then calculated from the areal proportion of quenched melt. The areal proportion of melt was determined from digitized pictures of the quenched samples by using the program NIH-Image [*Rasband*, 1997]. Strain contour diagrams of some samples were calculated from the displacement of the corundum particles using the program MARKER ANALYSIS [*Bons*, 1993; *Bons et al.*, 1993].

3. Melting Under Static Conditions

Static melting of a sample comprising 95% norcamphor and 5% benzamide was induced by rapidly increasing the temperature (2°C/min) from 38°C to 45°C, that is, to 3°C above the solidus of the norcamphor-benzamide aggregate. Melting initiated along the grain boundaries of neighboring

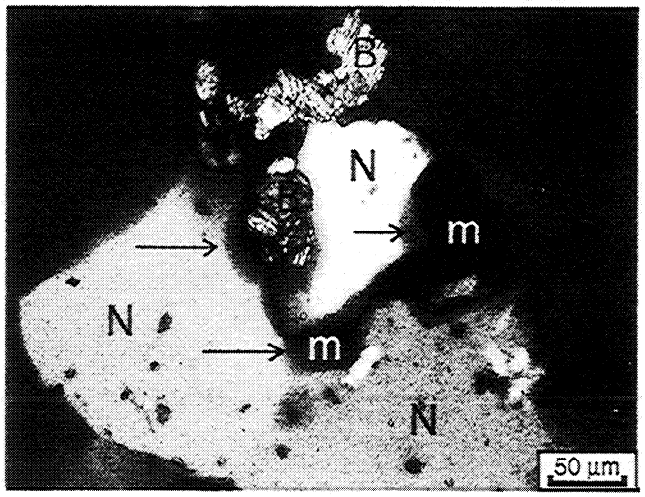

Figure 2. Appearance of first melt along norcamphor-benzamide grain boundaries in a sample melting under static conditions. N, norcamphor grains; B, benzamide grains; m, melt pockets and films. Black spots are corundum marker particles. Arrow points to a melt film along a norcamphor-benzamide grain boundary.

norcamphor and benzamide grains, as expected for a eutectic melt (e.g., see *Mehnert et al.*, [1973] for granitic rocks) and continued until the benzamide grains had entirely melted. We inferred the presence of melt from the appearance of shadows (observed in crossed polarized light) around the benzamide grains and along grain boundaries (arrow in Figure 2) and from the gradual disappearance of benzamide grains. With progressive melting, benzamide grains and part of the adjacent norcamphor grains were replaced by melt pockets (see "m" in Figure 2). These pockets are elliptically shaped, and therefore increase the surface area of the adjacent norcamphor grain boundaries. In this way, equilibrium norcamphor-benzamide boundaries are transformed into melt-norcamphor boundaries with different surface energies, thus leading to a new boundary configuration.

4. Melt-Free Deformation Experiments

To assess the effect of melt on the deformation mechanisms in our samples, we initially conducted melt-free experiments at a lower temperature (37°C) but at the same strain rates as in melting experiments. The temperature of 37°C corresponds to a homologous temperature of 0.83 for norcamphor, 0.76 for benzamide, and 0.98 for the norcamphor-benzamide aggregate. After a shear strain of $\gamma = 1$ a foliation defined by the long axes of norcamphor grains and benzamide grain aggregates developed at ~ 45° to the shear zone boundary. Norcamphor grains contain subgrains and deformation bands and undergo dynamic, grain boundary migration recrystallization. The average grain size increased to 200 µm, and the largest grains had long axes > 1 mm. A constant grain size was never attained. Together with the development of a crystallographic preferred orientation, these features indicate that dislocation creep is the dominant deformation mechanism in norcamphor. In contrast, benzamide grains show no evidence of intracrystalline plasticity. Rather, they form rigid clasts that passively rotate within the norcamphor matrix and eventually fracture along their cleavage planes. As shown below, synkinematic melting in the norcamphor-benzamide aggregate induces fracturing in norcamphor and modifies significantly the partitioning of strain on the granular scale.

Norcamphor and benzamide microstructures in these subsolidus experiments are similar to quartz and feldspar microstructures in high-temperature, greenschist to amphibolite facies mylonites (see Herwegh and Handy [1996] for a comparative study of norcamphor and quartz). It is therefore not surprising that many of the structures investigated in this paper are typical of anatectic quartzofeldspathic tectonites. We emphasize, however, that these structures are also found in many other partially molten crustal and mantle rocks.

5. Deformation Experiments in the Presence of Melt

Samples comprising 90 wt % norcamphor and 10 wt % benzamide, and 95 wt % norcamphor and 5 wt % benzamide were deformed continuously across the transition from subsolidus to hypersolidus conditions. In other words, after initial shearing to about $\gamma = 1$ in the absence of melting, the temperature was raised within 10 min from 37°C to 44-46°C during further deformation, such that the melt percentage increased progressively from 0 to ~ 15 vol % at finite shear strains of $\gamma \geq 0.5$.

Figure 3a shows that already at moderate shear strains ($\gamma = 2.3$) after the onset of melting, ~ 30% melt has left the partially-molten norcamphor-benzamide sample and accumulated between the PDMS and norcamphor frames, i.e., near the diametrically opposite, converging junctions of the norcamphor frame and frosted grips (Figure 3). The melt actually fills voids that open during shearing as the PDMS frame adheres to the glass plates and therefore separates from the norcamphor frame. This boundary condition induces rapid drainage of melt from the deforming norcamphor-benzamide aggregate, thereby allowing us to investigate syntectonic melt segregation patterns on the sample scale under drained conditions.

The presence of melt during deformation has a pronounced effect on the distribution of strain. Strain is more homogeneously distributed in melt-free samples, as shown in Plate 1. In the following, we relate the observed microstructural evolution of the samples during shearing to $\gamma = 1.6$ to strain contour diagrams (Plates 1 and 2) in order to illustrate how deformation localizes within the shear zone. The strain contour diagrams of Plates 1 and 2 were calculated for a sample consisting of 95 wt % norcamphor and 5 wt % benzamide, but the microstructural evolution of these samples and of those containing 10 wt % benzamide is basically the same. No melt escaped from the shear zone during this shear strain increment, and the area of the sample within the norcamphor frame did not vary with strain. This indicates that the volume of the norcamphor-benzamide aggregate within the shear zone remained nearly constant, at least until the melt started to accumulate outside of the shear zone between the norcamphor and PDMS frames. The strain contours in Plates 1 and 2 are therefore inferred to reflect true gradients in the local shear strain during bulk simple shearing to $\gamma = 1.6$. The following description is based on

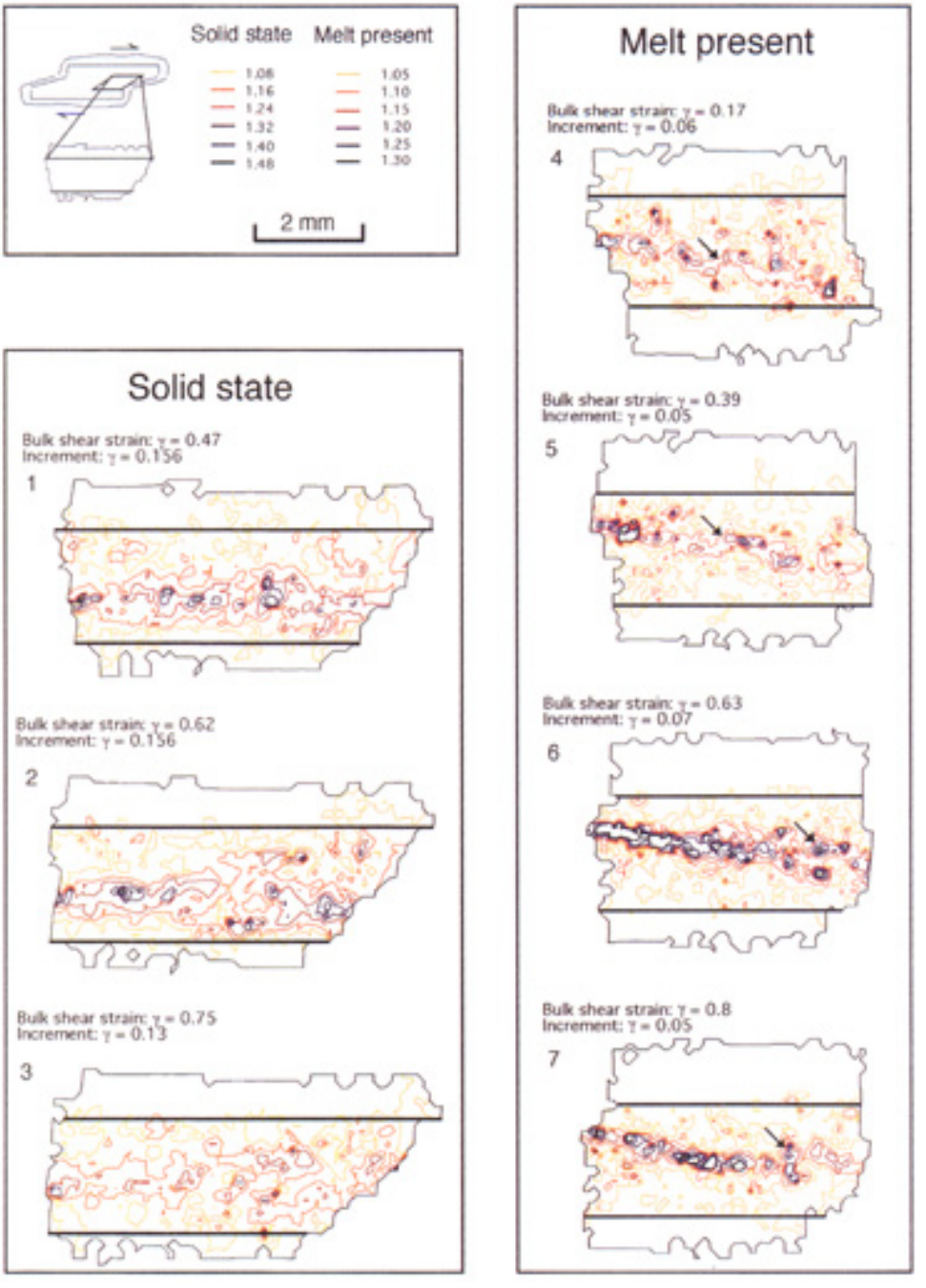

Plate 1. Sample consisting of 95 wt % norcamphor and 5 wt % benzamide. Finite strain analysis, with contours of the ratio of local to bulk strain [*Bons et al.*, 1993]. The contour diagrams correspond to different strain increments from the same experiment, which was run first in the absence of melt (stages 1 to 3) and then in the presence of melt (stages 4 to 7). The sample area in the strain analysis corresponds to the right edge of the sample and to about 1/3 of the area of the bulk shear zone (see inset). Solid horizontal lines represent shear zone boundaries. Stages 1, 2, and 3 are melt-free experiments, at $T = 37°C$. Strain contours calculated for strain intervals of $\gamma = 0.13$ and $\gamma = 0.15$ during simple shearing to $\gamma = 0.75$. Note that deformation is rather homogeneously distributed within the shear zone, with higher strain intensities in the middle to lower part of the shear zone. Stages 4, 5, 6, and 7 are experimental intervals during melting at $T = 46°C$. Same experiment and same part of the shear zone as illustrated in stages 1, 2, and 3. Strain contours calculated for shear strain intervals of approximately $\gamma = 0.05$ during simple shearing to $\gamma = 0.8$ after the onset of melting. Melting initiated after simple shearing to $\gamma = 0.75$ under subsolidus conditions. High strain areas at low angle to the shear zone boundary correspond to the melt-filled shear bands depicted in Figure 3 and Plate 2. Arrows point to high-strain, foliation-parallel areas that interconnect the shear bands.

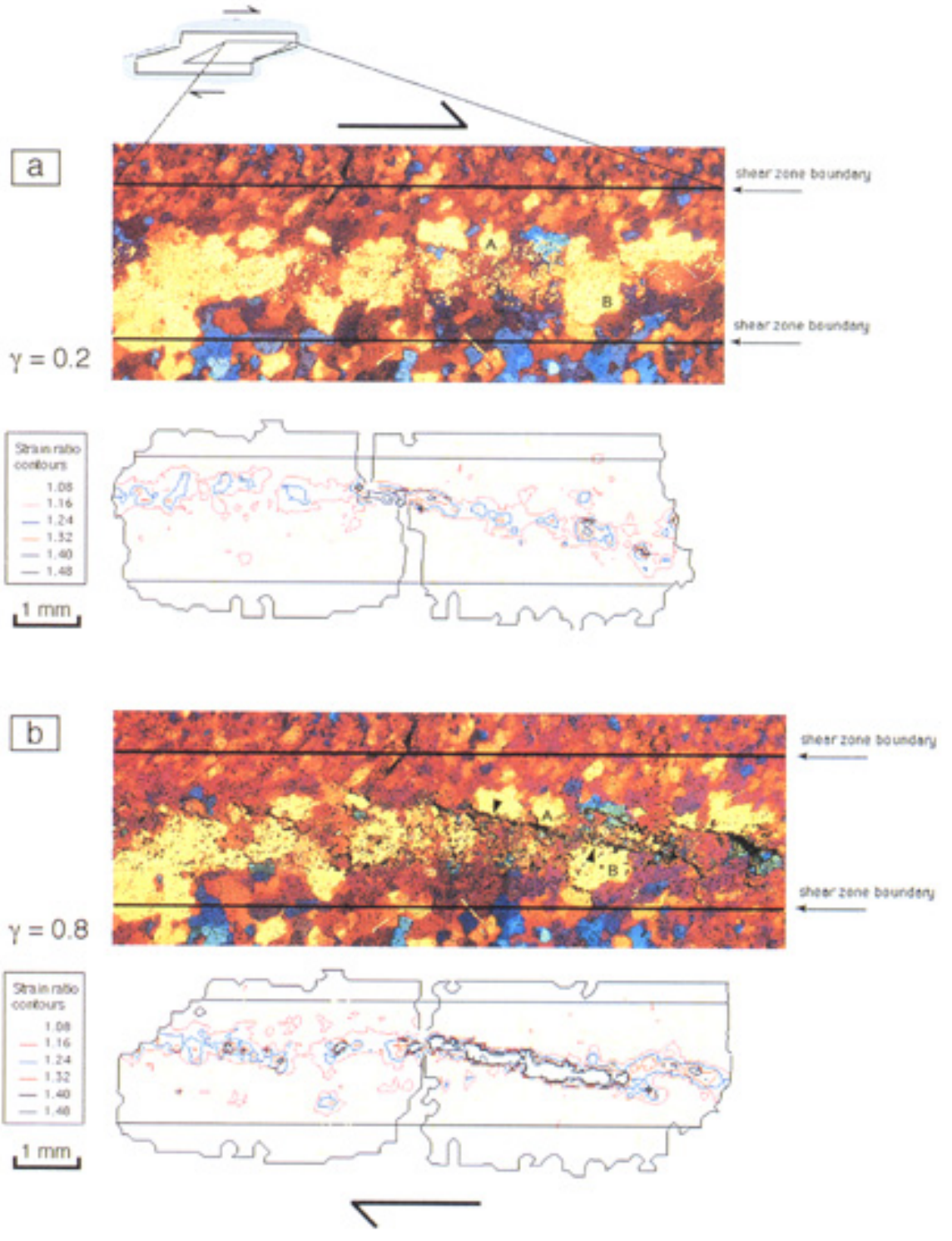

Plate 2. Microstructure observed with crossed polarizers and inserted gypsum plate and strain contour plots for photographed area. Letters A and B mark the grains that are displaced dextrally along a shear band during progressive deformation. (a) Shear strain of $\gamma = 0.2$ after the onset of melting. (b) Shear strain of $\gamma = 0.8$ after the onset of melting. Photograph was taken after quenching the sample. Dark surfaces (see arrowheads) oriented at a low angle to the shear zone boundaries are the quenched melt in the shear bands.

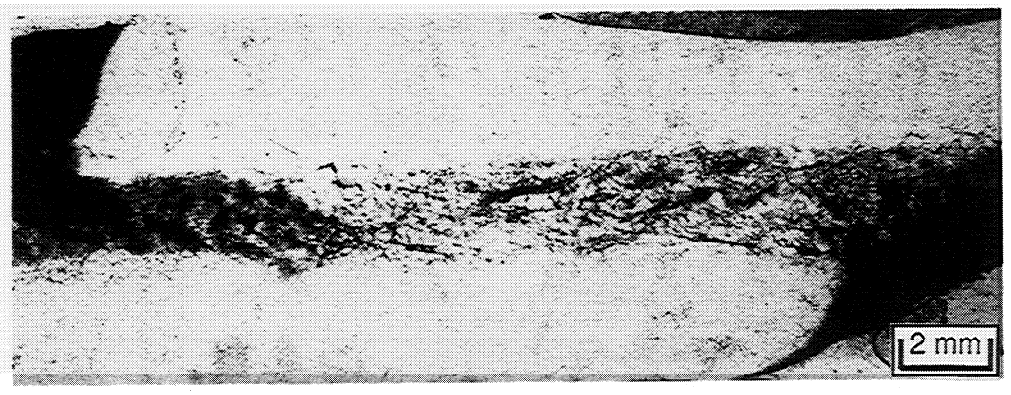

a

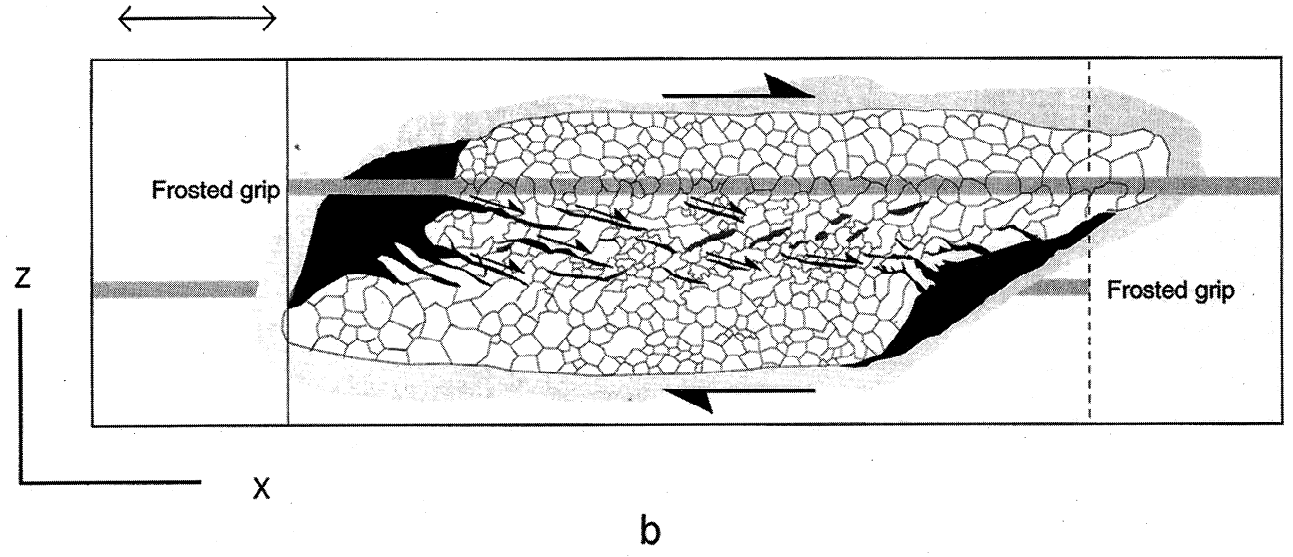

b

Figure 3. Sample consisting of 90 wt % norcamphor and 10 wt % benzamide, viewed in *XZ* plane after simple shearing to $\gamma = 3$, of which the final $\gamma = 2.3$ occurred during melting. (a) Sample viewed in plane polarized light. Dark microcrystalline aggregates (quenched melt) delimit melt-bearing shear bands. Note the accumulation of melt in voids that have opened at diametrically opposite ends of the sample, between the frames of norcamphor and PDMS. (b) Sketch of Figure 3a. Location of melt accumulation between frames of norcamphor and PDMS corresponds to black areas at both ends of the shear zone. Half arrows indicate dextral shear sense along melt-bearing shear bands. Dark gray areas represent unmelted benzamide aggregates that track the foliation plane. Double-headed arrow in top left corner indicates the displacement of the upper glass plate with respect to the fixed, lower glass plate.

one experiment. We emphasize, however, that the same microstructural evolution occurred in 10 other experiments.

The increase in temperature of 8°C which induces melting in the sample does not involve any change in the behavior of benzamide, which still forms rigid clasts that undergo rigid-body rotation in the norcamphor matrix. Recrystallization of norcamphor by grain boundary migration still occurs, but the average grain size of norcamphor becomes smaller than in the melt-free samples (150 μm instead of 200 μm).

Intergranular, melt-bearing extensional shear fractures (Figure 4) develop at the onset of melting even as the norcamphor in the rest of the sample undergoes pervasive dynamic recrystallization. Intergranular melt films on grain boundaries parallel to the ε_3 orientation are thicker (≤ 20 μm) than those oriented parallel to the ε_1 direction (Figure 4). *Dell'Angelo and Tullis* [1988] observed a similar melt distribution in experimentally deformed, partially molten aplite, during simultaneous dislocation creep and melt-induced fracturing. The geometry of the fractures combined with their appearance at the onset of melting suggests that they open in the presence of an overpressured melt (C. L. Rosenberg and M. R. Handy, manuscript in review, submitted to the Journal of Structural Geology, 1999).

After a shear strain increment of only $\gamma = 0.15$ from the onset of melting, shear bands form at both ends of the sample, as evidenced by the high-strain zones contoured in the deformation sequence of Plate 1 (stage 4). In addition, Plate 2 shows the dextral relative displacement on both sides of the shear band (compare positions of grains A and B of

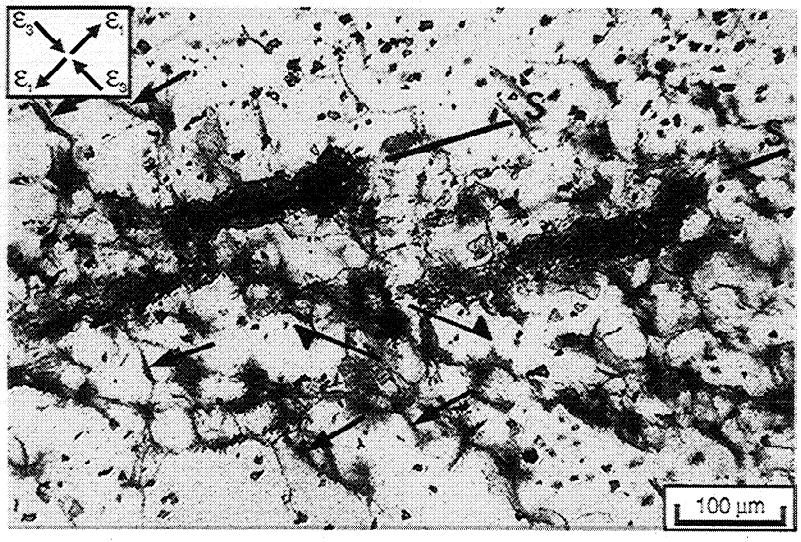

Figure 4. Detail of Figure 3a. Long side of micrograph is parallel to the shear zone boundary as viewed in the *XZ* fabric plane. Half arrows indicate the shear sense along a melt-bearing shear band. Small arrows point to melt-filled grain boundaries oriented subparallel to the incremental shortening direction ε_3. Dark, elongate aggregates defining S (foliation) are benzamide aggregates that were still unmelted when the sample was quenched. Solid dots are corundum particles that served as passive strain markers. Finite strain is $\gamma = 1.8$.

Plates 2a and 2b). These shear bands are zones of melt accumulation (Plate 2 and Figure 4) and we refer to them as "melt-bearing shear bands" because of their obvious geometric affinity with solid-state shear bands in mylonite [e.g., *Platt and Vissers*, 1980]. Initially (up to $\gamma = 0.2$ in the presence of melt), shear bands are relatively short (1-1.5 mm) and are oriented at a high angle (40°) to the shear zone boundary (see the high strain areas in stage 4 of Plate 1). This orientation corresponds approximately to that of melt-bearing grain boundaries aligned subparallel to the bulk, incremental shortening direction, ε_3, in the sample. As shown in stage 4 of Plate 1, the tips of shear bands were locally connected by foliation-parallel, high-strain zones (see arrows in Plate 1). Such foliation developed already during melt-free deformation.

With continued deformation ($\gamma = 0.4$ to 0.6) the melt-bearing shear bands increased in length and were oriented at a low angle (15°) to the shear zone boundary (see the high strain zones of stages 5 and 6 in Plate 1). Both strain localization and shear band interconnectivity increased with increasing strain (compare stages 4, 5, 6 and 7 of Plate 1). Melt accumulated within the shear bands, which appeared to be fed from melt-filled grain boundaries. In Figure 4, for example, the dextral, melt-bearing shear band (large half arrows) splays into several melt-filled grain boundaries (small arrows) that are oriented at higher angles (~ 45°) to the shear zone boundary than the shear band itself (~ 20°).

At shear strains higher than $\gamma = 0.7$ after the onset of melting, deformation becomes increasingly localized within the previously formed shear bands, as shown by the concentration of strain contours with higher values in Plate 2b compared to plate 2a. In addition, new shear bands nucleate in the central part of the sample (left part of Plate 2b), where deformation was rather homogeneously distributed up to shear strains of $\gamma = 0.6$ after the onset of melting (compare the left parts of Plates 2a and 2b). All shear bands are connected by foliation-parallel high-strain zones and form an interconnected layer throughout the entire shear zone (Plate 2b). The sequential development of the shear bands from the edge to the middle of the sample probably results from localization along the frosted grips forming the shear zone boundaries, as described by *Herwegh and Handy* [1998].

The melt percentage, grain size, and deformation mechanisms within the shear bands differ from those in the adjacent matrix (Figures 4 and 5 and Plate 3). At a shear strain increment of $\gamma = 0.8$ after the onset of melting, the areal proportions of melt are 0.15 within the bulk shear zone and 0.33 within the shear bands. In the matrix, norcamphor grains still undergo dynamic recrystallization by grain boundary migration. However, the average grain size of norcamphor decreases (150 µm, instead of 200 µm in the

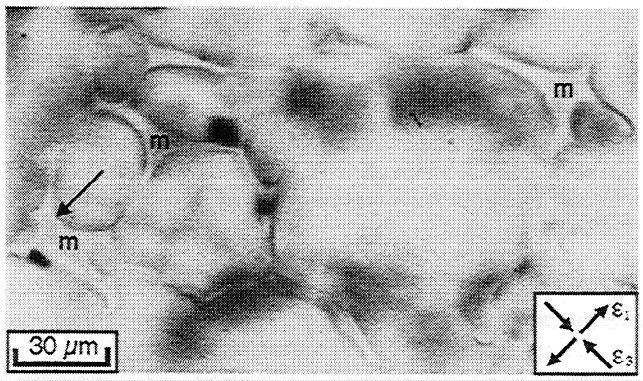

Figure 5. Microstructure in melt-bearing shear band. Arrow points to curved grain boundaries of rounded grains. Note melt pockets (m) with lengths oriented subparallel to the incremental shortening direction, ε_3. Finite strain is $\gamma = 1.61$ after the onset of melting.

absence of melt). In contrast, the average syntectonic grain size within the shear band is less than 100 μm (Plate 3). The grain size in the shear bands appears to remain constant with further deformation. Grain size reduction in the shear bands involves intragranular fracturing, combined with the nucleation and growth of tiny new norcamphor grains along the melt-filled fracture surfaces. The blue grain below marker 9 that appears in Plate 3d is a good example of this. The small grains within the melt-bearing shear bands tend to be equiaxed. Their boundaries are curved (arrow in Figure 5), lending them a rounded appearance. The grain aggregates in the shear bands have only a weak to negligible shape-preferred orientation. *Bussod and Christie* [1991] interpreted similar grain shapes in their experiments as evidence for abrasion during grain boundary sliding in the presence of melt. We found no evidence for abrasion at norcamphor grain boundaries, but grain boundary sliding is indeed the dominant deformation mechanism within the shear bands. This is documented in the microstructural sequence in Plate 3: the blue grains enclosing the corundum markers 13 and 22 slide past the yellow grain containing markers 10 and 11. The same sequence also shows evidence for dissolution at grain to grain contacts: the small blue grain to the left of marker 3 approaches the yellow grain containing markers 10 and 11 during progressive shearing. The area between these two grains disappears, and the distance between these markers decreases, even though these markers define a hypothetical line parallel to the local flow direction. Taken together, the microstructural evidence suggests that the dominant deformation mechanism in the melt-filled shear bands is melt-enhanced, diffusion-accommodated grain boundary sliding.

The differing deformation mechanisms in shear bands and matrix are associated with discernable differences in the melt distribution. In shear bands, melt pockets have smaller axial ratios and only a weak shape preferred orientation parallel to the flow direction, i.e., to the shear band boundary (compare Figures 4 and 5). Although deformation in the shear bands clearly occurs by grain boundary sliding, the corresponding melt configuration (Figure 5) is similar to that of olivine aggregates experimentally deformed in the presence of melt in the dislocation creep regime at high differential stresses [*Bussod and Christie*, 1991; *Daines*, 1997]. Our syntectonic melt distribution differs from that of the *Hirth and Kohlstedt* [1995a] experiments in which melt distribution during diffusion creep is not significantly different from that observed under static conditions. In the matrix, melt forms elongate grain boundary films (Figure 4) with a strong shape-preferred orientation subparallel to the incremental shortening direction. This shape-preferred orientation is similar to that described by *Zimmerman et al.* [1999] for partially molten mantle rocks deformed in simple shear.

The successive appearance of melt first in pockets and continuous films along dilatant grain boundaries, then within extensional shear fractures, and finally as accumulations outside of the shear zone indicates that melt leaves the sample during deformation. At low to moderate shear strains the melt-bearing shear bands terminate at the frosted grips, whereas at higher shear strains the shear bands propagate into, and even transect, the norcamphor frame at either end of the aggregate (Figure 3). The inferred flow of melt from the matrix grains between the shear bands into the shear bands themselves is consistent with the observed strain distribution patterns: The constant sample volume during shearing to $\gamma = 1.6$, together with the observation that the extensional shear fractures are always filled with melt, suggests that dilation in domains of fracturing is compensated by a volume decrease of material between the fractures. It is reasonable to assume that this local volume deficit corresponds to the amount of melt drained along grain boundaries into the fractures.

The syntectonic melt pressure in the partially molten norcamphor-benzamide aggregate is certainly higher than in the norcamphor frame; otherwise, melt would not be expelled to initially melt-free regions outside of the norcamphor-benzamide aggregate. Because we were unable to measure melt pressure in different parts of the sample, however, we were unable to determine whether the melt pressure in the sample exceeded the atmospheric confining pressure (thus expelling melt from the aggregate), or whether the voids represent underpressured regions that effectively sucked the melt from the sample. In either case, the sequential development of dilatant grain boundaries and melt-bearing shear bands indicates that melt migrated down a melt-pressure gradient.

What evidence is there for the former presence of a melt in the shear bands after that melt has crystallized? To answer this question, we conducted a series of experiments without quenching the samples at the end of deformation. Instead, we decreased the temperature slowly (1°C/h) from 46°C (the temperature of shearing) to 40°C (i.e., 2°C below the solidus temperature) under static conditions until the melt was completely crystallized. New grains did not nucleate from the intergranular melt in the shear bands. Rather, they grew in crystallographic continuity with the matrix grains lining the melt-filled shear band (Fig 6b). The following microstructures that are diagnostic of a crystallized melt were preserved after deformation and crystallization ended: (1) grain boundaries of norcamphor grains partly retained their alignment parallel to the previously melt-filled shear band (Figure 6b); and (2) small, elongate benzamide grains that had passively rotated into the shear band remained oriented with their long axes parallel to the shear band and grew to a larger size (e.g., grain 3 in Figure 6). We did not observe any of the commonly used criteria for identifying the former presence of melt in natural rocks [e.g., *Vernon and Collins*, 1988], such as euhedral grain aggregates of eutectic composition or interstitial films of one phase (e.g., benzamide) surrounding residual grains of another phase (e.g., norcamphor). The latter has occasionally been observed in natural migmatites [e.g., *Carson et al.*, 1997; *Brown et al.*, 1999; *Sawyer*, 1999; *Rosenberg and Riller*, 2000]. The crystallization of such an interstitial phase requires the absence of grains of this same phase in its direct vicinity. As can be seen in Figure 6, grains of both phases (benzamide and norcamphor) are still present in close vicinity of the melt bearing shear band. Melt crystallized on these existing grains rather than nucleating new grains in the interstices.

6. Discussion

The above results may have implications for melt segregation processes in naturally deformed rocks. To focus the discussion below, we discuss our results in the context of several questions at the heart of current debates on magma tectonics.

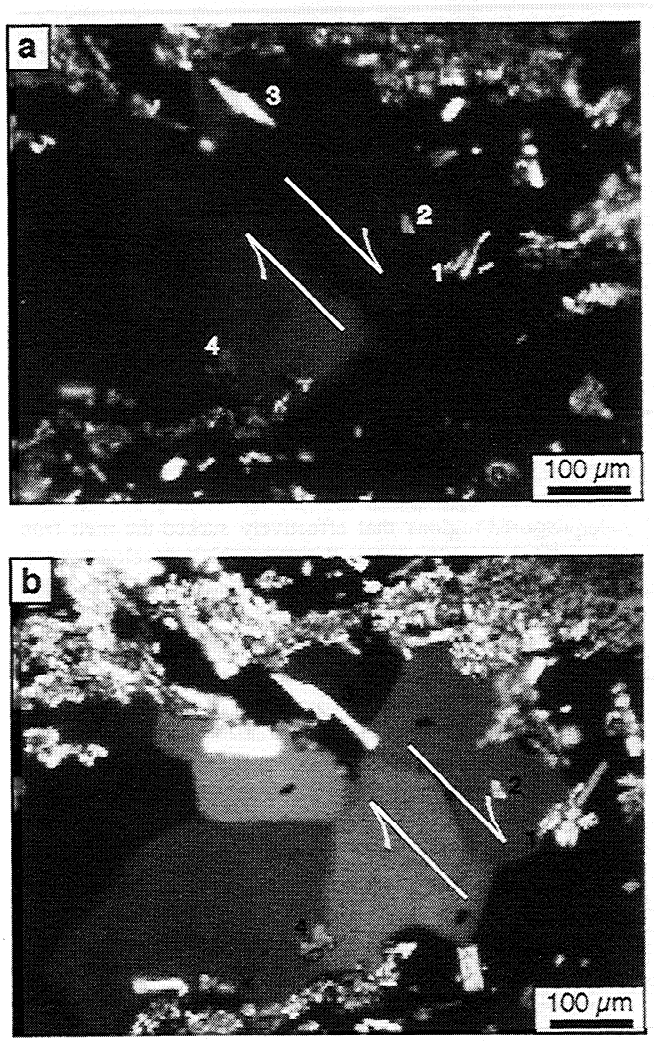

Figure 6. Microstructure of a melt-bearing shear band (a) during syntectonic melting and (b) after complete crystallization. Numbers refer to benzamide grains that can be identified in both photos. Half arrows indicate shear sense and location of shear band. Note the melt channel (black) parallel to and between the arrows in Figure 6a. See text for further details.

6.1. Are the Microstructures and Processes in Our See-through Experiments Typical of Those Inferred for Syntectonic Anatexis in Naturally Deforming Rocks?

The results in this paper only shed light on melt segregation mechanisms in rocks if the experimental and natural microstructures are sufficiently alike to allow one to infer common, underlying processes. The partially molten norcamphor-benzamide aggregates showed several grain-scale features found in natural, anatectic rocks that are inferred to have undergone deformation in the presence of < 20 vol % of melt [*Rosenberg and Riller*, 2000]: (1) The matrix grains in our experiments (norcamphor) and in gneissic rocks (quartz) underwent dynamic, grain boundary migration recrystallization in the presence of a melt; and (2) The melt is distributed along the grain boundaries, preferentially along boundaries that are initially oriented at a high angle to the foliation. Our experiments also showed a strain- and melt-percentage-dependent switch in the predominant deformation mechanism from dislocation creep at high homologous temperatures and dry conditions to combined dislocation creep and fracturing in the presence of melt. This mechanistic transition was also documented in triaxial deformation experiments on partially molten aplites [*Dell'Angelo and Tullis*, 1988] and inferred in naturally deformed, anatectic rocks [e.g., *Rosenberg and Riller*, 2000].

Regarded on a larger scale, the melt-filled shear bands in our drained, simple shear experiments have natural counterparts: Shear bands and shear zones containing crystallized melt are ubiquitous in migmatitic terranes [e.g., *Brown*, 1994] and these structures are often cited as evidence for coeval melting and shearing [e.g., *Vauchez and Egydio da Silva*, 1992; *Rey et al.*, 1992]. The contiguity of melt-bearing shear bands with low-pressure accumulation sites as observed in our experiments is rarely found on the grain and outcrop scales in nature but is observed on the map scale where plutons are adjacent to or within shear zones [e.g., *Hutton*, 1982]. All of these microstructural similarities suggest that the see-through experiments described above reproduce many of the melt segregation processes operating in nature, even if the formation of many melt-related microstructures in both nature and experiment is still not fully understood (see discussion below).

Similarity of natural and experimental microstructures should not be taken to imply that the experiments are necessarily scaled to natural viscosities, temperatures, and pressures. *Park and Means* [1996] observed that deformation mechanisms in their anatectic, rock analogue experiments were rate-dependent. Decreased strain rate and differential stress induced a transition in the dominant deformation mechanism from dislocation creep to contact melting and grain boundary sliding. In our experiments, melting and melt segregation are intimately related to these same deformation mechanisms and may therefore also be highly non linear, rate-dependent processes. In this context, we note that the melt volumes segregated in our experiments are large on the lengthscale and timescale of deformation in the samples (~ 30% after a shear strain of $\gamma = 2.3$; see Figure 3). What little is known about melt segregation rates, however, suggests that such rates are also high in nature: *Sawyer* [1991] estimates segregation rates of tonalitic melts of the Grenville Front to be faster than 2 cm/yr.

In fact, we can estimate the scaling factors for melting and strain rates in our experiments. Approximately 5 hours at 45°C were employed to melt 15 vol % of the norcamphor-benzamide aggregate, during which time the aggregate undergoes a shear strain of $\gamma = 0.5$. In nature, an estimated 0.5 Myr is required to melt 15 vol % of a crustal protolith once the ambient P-T conditions for melting have been attained [e.g., *Patiño Douce et al.*, 1990]. Therefore the melting rates in our analogue experiments are about 10^9 times faster than natural melting rates. This same factor (10^9) is needed to scale the experimental strain rates of this study (10^{-5} s^{-1}) to natural strain rates, if one assumes the latter to be of the order of 10^{-14} s^{-1} [e.g., *Pfiffner and Ramsay*, 1982]. Therefore the ratio of melting rate to strain rate in our experiments is consistent with that expected in nature. In the experiments, melt-bearing shear bands form after a shear strain increment of only $\gamma = 0.2$ in the presence of a melt, corresponding to a natural time of only 0.6 Myr. Therefore

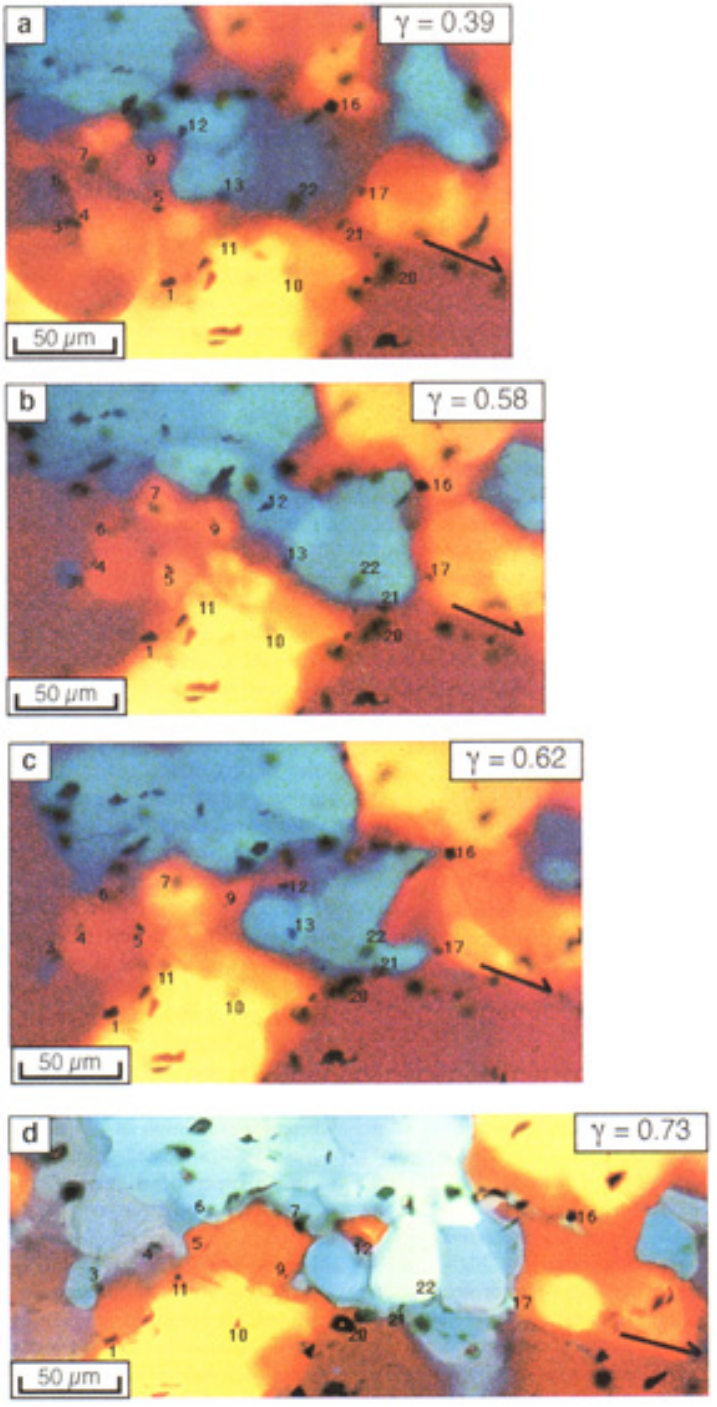

Plate 3. Microstructural evolution of norcamphor and benzamide grains within a shear band during syntectonic melting. Numbers refer to corundum marker particles (dots) mentioned in the text. Half arrow indicates local flow direction of solid grains in the shear band.

the transition from homogeneous to highly localized deformation is expected to follow the onset of melting very quickly.

6.2 Does Melting Localize Deformation or Does Deformation Localize Melt Flow?

In attempting to answer this chicken-or-egg question, people have proposed several models for the formation of melt-filled shear zones: (1) intrusion of melt along a preexisting shear zone [*Vauchez and Egydio da Silva*, 1992; *Kelemen and Dick*, 1995]; (2) penetration of hydrous metamorphic fluids into a preexisting shear zone, thereby lowering the solidus of the rock and inducing melting within narrow envelopes adjacent to the shear zones [*Mogk*, 1992]; and (3) nucleation of shear zones at preexisting melt pockets or other sites of accumulated melt [*Grujic and Mancktelow*, 1998]. Models 1 and 2 require that localized shearing predate melting, whereas in model 3 melting predates localized shearing and the predeformational melt distribution controls subsequent localization.

In contrast to these models, our experiments indicate that strain localization within the shear zone occurs only when melting begins. As illustrated in Plate 1, the nucleation of shear bands is nearly contemporaneous with the onset of melting. Melt is then channelled into the shear bands during their propagation. A remarkable finding in our simple shear experiments is that shear bands are mainly sites of melt transport. The melt originates on the grain boundaries throughout the matrix grains and is then either squeezed or sucked into the shear bands. Once in the shear bands, the melt is expelled down the melt pressure gradient to the edges of the deforming norcamphor-benzamide aggregate. Thus shear bands fulfill a dual kinematic and dynamic role. As structural and mechanical heterogeneities, they alleviate local strain incompatibilities introduced by partial melting and intragranular fracturing. As melt conduits, they relieve differences in melt pressure between the deforming source region and the less deformed or undeformed sink region.

6.3. What is the Effect of Heterogeneous Melt Distribution on the Attainment of the RCMP?

Experimental studies on the deformation of partially molten granite [*Arzi*, 1978; *Van der Molen and Paterson*, 1979] suggested that the drop in viscosity from that of a solid rock to that of a liquid occurs over a restricted range of melt fractions ranging from 0.1 to 0.3 [*Arzi*, 1978]. *Arzi* [1978] termed this range the "rheological critical melt percentage" or RCMP. *Van der Molen and Paterson* [1979] suggested that the above transition occurs at higher melt fractions. They inferred that the maximum rate of decrease in strength with increasing melt fraction occurs at melt fractions between 0.30 and 0.35. In our experiments the maximum melt fractions in the samples as a whole (0.1 to 0.15) barely attained the RCMP. This is consistent with *Brown and Rushmer*'s [1997] prediction that melt migration out of naturally deformed rock prevents the melt from ever becoming sufficiently abundant to attain the RCMP. However, melt fractions within the shear bands (0.2 to 0.3) do attain the RCMP. Strain localization is therefore associated with local attainment of the RCMP and presumably with a related drop in the strength/viscosity of the sample as a whole.

6.4 What Are the Effects of Melt Segregation on Bulk Rock Rheology?

Insomuch as microstructures are indicative of deformation mechanisms and rheology, they can be used to infer how melting affects the rheology of partially molten rocks. On the basis of the microstructural changes described above, we propose the following strain-dependent rheological evolution for deforming anatectic rocks (Figure 7): Because melt under pressure counteracts normal stresses acting across grain boundaries [*Shaw*, 1980], it induces hydrofracturing (Figure 7a) and thus relaxes strain incompatibilities within the deforming aggregate. The formation of intergranular fracture networks allows the melt to permeate the aggregate very quickly and to coat the boundaries of grains which line the shear fractures. The alignment of several favourably oriented, melt-coated grain boundaries allows the grains to slide past each other and thus to nucleate shear bands (Figure 7b). As *Cooper and Kohlstedt* [1984] showed, a thin film of melt along grain boundaries probably provides an efficient diffusional pathway that accommodates grain boundary sliding, even in fairly coarse grained (> 0.5 mm) aggregates.

A strain-dependent switch from dislocation creep to diffusion-accommodated grain boundary sliding in the melt-filled shear bands (Figure 7c) is expected to reduce significantly the bulk strength of the norcamphor-benzamide aggregate, as has been inferred from numerous rock deformation experiments. *Jin et al.* [1994] speculated that pervasive, viscous grain-boundary sliding in the presence of melt was responsible for a strain-dependent drop in the strength of synthetic peridotites that had been undergoing dislocation creep. *Hirth and Kohlstedt* [1995b] attributed an order of magnitude increase in the creep rate of olivine aggregates deforming at melt percentages larger than 4 vol % to the onset of viscous grain boundary sliding. Therefore, because melt-bearing shear bands form interconnected weak layers in our samples (Figure 7d), they may reduce the strength of the aggregate significantly, even though they make up only a modest proportion of the total aggregate volume. As pointed out above, melt percentages in the shear bands attain the RCMP. The magnitude of the strength drop associated with the interconnection of the shear bands is difficult to ascertain. It is probably less than that recorded by *Arzi* [1978] and *Van der Molen and Paterson* [1979] because their experiments occurred entirely under brittle conditions, whereas deformation in our shear bands occurred mainly by diffusion-accomodated grain boundary sliding.

In our experiments, melt migrated from the matrix, which is inferred to be stronger, to the shear bands, which are inferred to be weaker. *Rutter* [1997] suggested that melt migrates down pressure gradients from the stronger to the weaker layers of deforming rocks. The pressure gradient in this model is actually a gradient in mean stress which results from the assumption that the strain rate is uniform in all parts of the deforming aggregate. Our experiments, however, indicate that the strain rate in the shear bands is about 1.2 to 1.5 times higher than that of the adjacent matrix. *Stevenson* [1989] showed that melt migrates toward regions that are already enriched in melt, thus preferentially increasing the melt content of areas whose melt volume proportion is already higher. Although we could not test this model adequately, we feel that some combination of the two models explains the melt migration patterns in our experiments: Melt flows from intergranular fractures within a stronger,

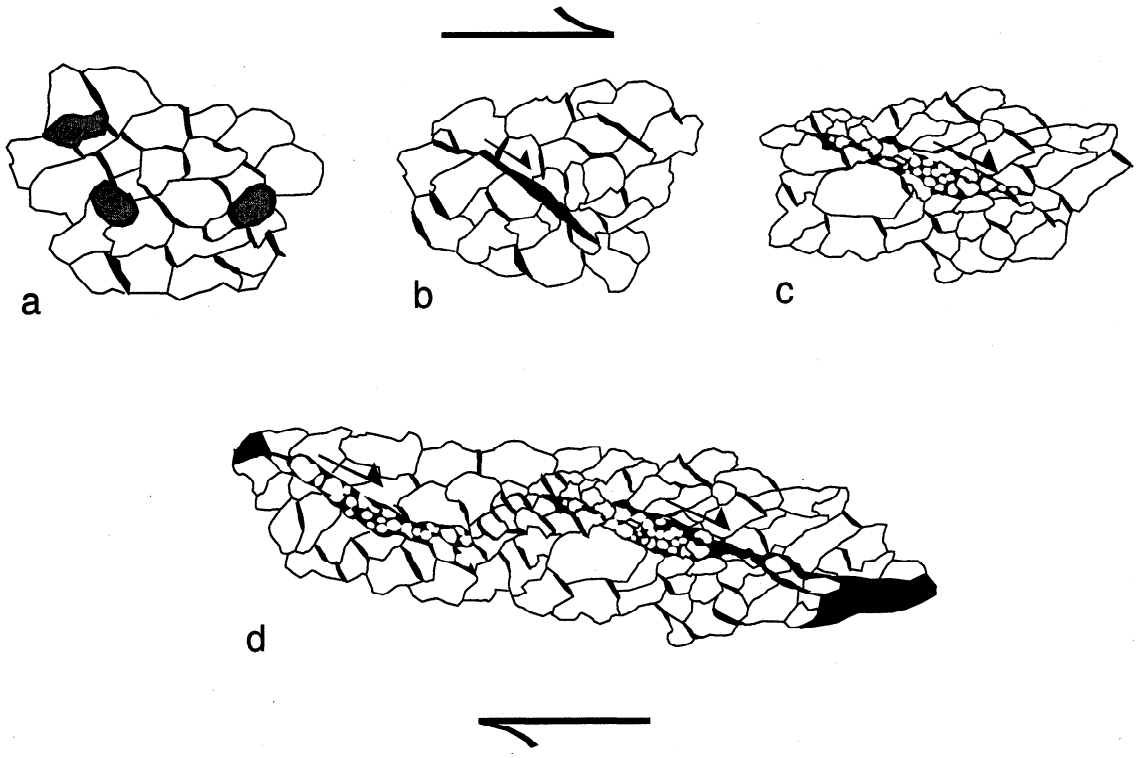

Figure 7. Schematic model of nucleation and growth of melt-bearing shear bands during progressive simple shear. Solid, melt; shading, benzamide; open, norcamphor. (a) Melt is initially distributed at norcamphor-benzamide grain boundaries and along intergranular fractures subparallel to the incremental shortening direction. Where melt-filled grain boundaries are aligned along several grains (b), shear bands nucleate at a high angle to the shear zone boundary. With progressive deformation melt-bearing shear bands become more elongate (c) and are oriented at lower angle to the shear zone boundary. At this stage a switch in the deformation mechanisms from dislocation creep and intergranular fracturing to diffusion-accommodated grain boundary sliding has taken place within the shear bands. At higher shear strain melt-bearing shear bands form an interconnected weak layer along the entire shear zone (d). Shear bands channel the melt from grain boundaries to the edge of the sample, where it accumulates between the norcamphor and PDMS frames.

slowly deforming matrix to dilatant, melt-filled shear bands deforming at higher strain rates.

7. Conclusions

Shear bands in partially melting aggregates develop after only small strains and short times in the presence of a melt. Melt-bearing shear bands fulfill several roles relating both to the bulk rheology and to the distribution of melt. In forming interconnected surfaces subparallel to the shearing plane, they weaken the aggregate, especially when the dominant deformation mechanism in the shear bands switches from dislocation creep to diffusion-accommodated grain boundary sliding. As discrete interconnected channels, the shear bands also serve as melt conduits, channeling melt from source regions at higher melt pressures to sinks at lower melt pressure. Only in the shear bands does the melt percentage attain the RCMP. With progressive deformation, permeabilty becomes highly anistropic, with melt migrating down melt pressure gradients within the shearing plane. The flow of overpressured melt through a network of active shear bands within a solid, deforming framework contrasts with previous models of melt porosity in which melt moves through an interconnected network of constantly opening and closing fractures [e.g., *Rutter*, 1997]. In this context, we emphasize that deformation and melt segregation are fully ductile processes on the scale of the aggregate. Fracturing is restricted to the granular scale and predominates only at the onset of deformation in the presence of a melt.

The role of melt during deformation is twofold: First, it induces a pore fluid pressure, which reduces the effective strength of the aggregate and induces intergranular fracturing. Dilation associated with fracturing is what creates the grain-scale pathways that allow the melt to drain from the dynamically recrystallizing matrix into the shear bands. Second, melt is the diffusive medium that facilitates diffusion-accommodated grain boundary sliding within the shear bands themselves.

Our experiments indicate that once the melt crystallizes, only locally do microstructural traces betray former melt migration. All traces of the melt are obliterated if deformation continues below the solidus, a history which is expected of many retrograde shear zones. Despite the weakness of organic analogue materials, melting rate scales realistically with strain rate in our experiments, allowing one to draw semiquantitative conclusions about the relationship between deformational and magmatic processes in nature.

Acknowledgments. Marco Herwegh (Bern), Mathias Hafner (Mainz), and Bas den Brok (Zürich, formerly Mainz) eased the introduction of one of us (C.R.) to see-through experimental deformation of rock analogues. Our technicians, Kurt Bürger, Thomas Ramsch, and Manfred Kern (Giessen) constructed and improved the experimental apparatus. Peter Bauer (Giessen) and Jürgen Streit (ANU, formerly Giessen), shared the travails of many failed experiments and made numerous helpful suggestions. In particular, Peter Bauer is acknowledged for many discussions and for his help with solving technical problems. We thank all of the above for their support and encouragement. We also acknowledge the careful reviews of the journal reviewers, Mike Brown and Jan Tullis, the JGR Associate Editor Michael Walter, Win Means, and Y. Park. This work was carried out with the financial support of the the German Science Foundation in the form of DFG-project IIa-2403/2 (SPP "Orogene Prozesse...").

References

Arbaret, L., H. Diot, and J. L. Bouchez, Shape fabrics of particles in low concentration suspensions: 2D analogue experiments and application to tiling in magma, *J. Struct. Geol., 18*, 941-950, 1996.

Arzi, A. A., Critical phenomena in the rheology of partially melted rocks, *Tectonophysics, 44*, 173-184, 1978.

Bauer, P., C. L Rosenberg, and M. R. Handy, Deformation experiments on rock-analogue materials at controlled confining pressure: A new approach for studying strain localization at the brittle to viscous transition, *J. Struct. Geol.,* in press, 2000.

Bons, P., *Experimental deformation of polyphase rock analogues*, 207 pp. 207, Geologica Ultrajectina, vol. 110, Utrecht, 1993.

Bons, P. D., M. W. Jessel, and C. W. Passchier, The analysis of progressive deformation in rock analogues, *J. Struct. Geol., 15*, 403-411, 1993.

Brown, M., The generation, segregation, ascent and emplacement of granite magma: The migmatite-to-crustally-derived granite connection in thickened orogens, *Earth Sci. Rev., 36*, 83-130, 1994.

Brown, M., and T. Rushmer, The role of deformation in the movement of granitic melt: Views from the laboratory and the field, in *Deformation-Enhanced Fluid Transport in the Earth's Crust and Mantle. Mineral. Soc. Ser., vol.* 8, edited by M. B. Holness, pp. 111-144, Chapman and Hall, New York, 1997.

Brown, M. A., M. Brown, W. D. Carlson, and C. Denison, Topology of syntectonic melt flow networks in the deep crust: Inferences from three-dimensional images of leucosome geometry in migmatites, *Am. Mineral., 84*, 1793-1818, 1999.

Bussod, G. Y., and J. M. Christie, Textural development and melt topology in spinel lherzolite experimentally deformed at hypersolidus conditions, *J. Petrol., Special lherzolite Issue*, 17-39, 1991.

Carson, C. J., R. Powell, C. J. L. Wilson, and P. H. G. M. Dirks, Partial melting during tectonic exhumation of a granulite terrane: an example from the Larsemann Hills, East Antarctica, *J. Metamorph. Geol., 15*, 105-126.

Cesare, B., E. Salvioli Mariani, and G. Venturelli, Crustal anatexis and melt extraction during deformation in the restitic xenoliths at El Joyazo (SE Spain), *Mineral. Mag. 61*, 15-27, 1997.

Collins, W. J., and E. W. Sawyer, Pervasive magma transfer through the lower-middle crust during non-coaxial compressional deformation: An alternative to diking, *J. Metamorph. Geol., 14*, 565-579, 1996.

Cooper, R.F., and D. L. Kohlstedt, Solution-precipitation enhanced diffusional creep of partially molten olivine-basalt aggregates during hot-pressing, *Tectonophysics, 107*, 207-233, 1984.

Daines, M. J., Melt distribution in partially molten peridotites: Implications for permeability and melt migration in the upper mantle, in *Deformation-Enhanced Fluid Transport in the Earth's Crust and Mantle. Mineral. Soc. Ser., vol.* 8, edited by M. B. Holness, pp. 62-81, Chapman and Hall, New York, 1997.

Davidson, C., L. S. Hollister, and S. M. Schmid, Role of melt in the formation of a deep-crustal shear zone: The Maclaren Glacier metamorphic belt, south central Alaska, *Tectonics, 11*, 348-359, 1992.

Dell'Angelo, L. N., and J. Tullis, Experimental deformation of partially melted granitic aggregates, *J. Metamorph. Geol., 6*, 495-515, 1988.

Grujic, D., and N. Mancktelow, Melt bearing shear zones: analogue experiments and comparison with examples from southern Madagascar, *J. Struct. Geol., 20*, 673-689, 1998.

Hartel, T. H. D., and D. R. M. Pattison, Genesis of the Kapuskasing (Ontario) migmatitic mafic granulites by dehydration melting of amphibole: The importance of quartz to reaction progress, *J. Metamorph. Geol., 14*, 591-611, 1996.

Herwegh, M., and M. R.. Handy, The evolution of high-temperature mylonitic microfabrics: Evidence from simple shearing of a quartz analogue (norcamphor), *J. Struct. Geol., 18*, 689-710, 1996.

Herwegh, M., and M. R. Handy, The origin of shape preferred orientations in mylonite: Inferences from in-situ experiments on polycrystalline norcamphor, *J. Struct. Geol., 20*, 681-694, 1998.

Hirth, G., and D. L. Kohlstedt, Experimental constraints on the dynamics of the partially molten upper mantle: Deformation in the diffusion creep regime, *J. Geophys. Res., 100*, 1981-2001, 1995a.

Hirth, G., and D. L. Kohlstedt, Experimental constraints on the dynamics of the partially molten upper mantle 2, Deformation in the dislocation creep regime, *J. Geophys. Res., 100*, 15441-15449, 1995b.

Hollister, L. S. and Crawford, M. L., Melt enhanced deformation: A major tectonic process. *Geology,* 558-561, 1986.

Hutton, D. H. W., A tectonic model for the emplacement of the Main Donegal Granite, NW Ireland, *J. Geol. Soc. London., 139*, 615-631, 1982.

Ildefonse, B., and N. S. Mantckelow, Deformation around rigid particles: The influence of slip at the particle/matrix interface, *Tectonophysics, 221*, 345-359, 1993.

Ildefonse, B., L. Arbaret, and H. Diot, Rigid particles in simple shear flow: is their preferred orientation periodic or steady-state?, in *Granite: From Segregation of Melt to Emplacement Fabrics*, edited by J. L. Bouchez, D. H. W. Hutton, and W. E. Stephens, pp. 177-185, Kluwer Acad., Norwell, Mass., 1997.

Jin, Z., H. W., Green, and Y. Zhou, Melt topology in partially molten mantle peridotite during ductile deformation, *Nature, 372*, 164-167, 1994.

Kelemen, P. B., and J. B. Dick, Focused melt flow and localized deformation in the upper mantle: Juxtaposition of replacive dunite and ductile shear zones in the Josephine peridotite, SW Oregon, *J. Geophys. Res., 100*, 423-438, 1995.

Kohlstedt, D. L., and M. E. Zimmerman, Rheology of partially molten mantle rocks, *Ann. Rev. Earth Planet. Sci., 24*, 41-62, 1996.

Laporte, D., C. Rapaille, and A. Provost, Wetting angles, equilibrium melt geometry, and the permeability threshold of partially molten crustal protholiths. in *Granite: From Segregation of Melt to Emplacement Fabrics*, edited by J. L. Bouchez, D. H. W. Hutton, and W. E. Stephens, pp. 31-54, Kluwer Acad., Norwell, Mass., 1997.

Means, W. D., A deformation experiment in transmitted light, *Earth Planet. Sci. Lett., 35*, 169-179, 1977.

Means, W. D., Synkinematic microscopy of transparent polycrystals, *J. Struct. Geol., 11*, 163-174, 1989.

Mehnert, K.R., W. Büsch, and G. Schneider, Initial melting at grain boundaries of quartz and feldspar in gneisses and granulites, *Neues Jahrb. Mineral. Monatsh. 4*, 165-183, 1973.

Mogk, D. W., Ductile shearing and migmatization at mid-crustal levels in an Archean high-grade gneiss belt, northern Gallatin Range, Montana, USA, *J. Metamorph. Geol., 10*, 427-438, 1992.

Nicolas, A., A melt extraction model based on structural studies in mantle peridotites, *J. Petrol., 27*, 999-1022 1986.

Park, Y., and W. D. Means, Direct observation of deformation processes in crystal mushes, *J. Struct. Geol., 18*, 847-858, 1996.

Patiño Douce, A. E., E. D. Humphreys, and D. A. Johnston, Anatexis and metamorphism in tectonically thickened continental crust exemplified by the Sevier hinterland, western North America, *Earth Planet. Sci. Lett., 97*, 290-315, 1990.

Pfiffner, O. A., and J. G. Ramsay, Constraints on geological strain rates, arguments from finite strain states of naturally deformed rocks, *J. Geophys. Res., 87*, 311-321, 1982.

Platt, J. P. and R. L. M. Vissers, Extensional structures in anisotropic rocks, *J. Struct. Geol., 2*, 397-410, 1980.

Rasband, W., Image 1.61, Nat. Inst. of Health, Res. Serv. Branch NIMH, Bethesada, Md., 1997.

Rey, P., J. P. Burg, and J. M. Caron, Middle and Late Carboniferous extension in the Variscan Belt: Structural and petrological evidences from the Vosges massif (eastern France), *Geodin. Acta, 5*, 17-36, 1992.

Rosenberg, C. L., and U. Riller, Partial-melt topology in statically and dynamically recrystallized granite, *Geology*, in press, 2000.

Rutter, E. H., The influence of deformation on the extraction of crustal melts: A consideration of the role of melt-assisted granular flow. in *Deformation-Enhanced Fluid Transport in the Earth's Crust and Mantle. Mineral. Soc. Ser., vol.* 8, edited by M. B. Holness, pp. 82-110, Chapman and Hall, New York, 1997.

Sawyer, E. W., Disequilibrium melting and the rate of melt-residuum separation during migmatization of mafic rocks from the Grenville Front, Quebec., *J. Petrol., 32*, 701-738, 1991.

Sawyer, E., W., Criteria for the recognition of partial melting, *Phys. Chem. Earth*, 24, 269-279, 1999.

Shaw, H. R., Fracture mechanisms of magma transport from the surface. in *Physics of magmatic processes*, edited by R. B. Hargraves, pp. 201-264, Princeton Univ. Press, Princeton, N.J., 1980.

Stevenson, D. J., Spontaneous small-scale melt segregation in partial melts undergoing deformation, *Geophys. Res. Lett., 16*, 1067-1070, 1989.

Van der Molen, I., and Paterson M. S., Experimental deformation of partially-melted granite, *Contrib. Mineral. Petrol., 70*, 299-318, 1979.

Vauchez, A., and M. Egydio da Silva, Termination of a continental-scale strike-slip fault in partially melted crust: The West Pernambuco shear zone, northeast Brazil, *Geology, 20*, 1007-1010, 1992.

Vernon, R. H., and W. J. Collins, Igneous microstructures in migmatites, *Geology, 16*, 1126-1129, 1988.

Weijermars, R., Flow behaviour and physical chemistry of bouncing putties and related polymers in view of tectonic laboratory applications, *Tectonophysics, 124*, 325-358, 1986.

Zimmerman, M. E., S. Zhang, D. L. Kohlstedt, and S. Karato, Melt distribution in mantle rocks deformed in shear, *Geophys. Res. Lett., 26*, 1505-1508, 1999.

C. L. Rosenberg and M. R. Handy, Institut für Geowissenschaften, Justus Liebig Universität Giessen, Senckenbergstrasse 3, D-35390 Giessen, Germany. (Claudio.L.Rosenberg@geolo.uni-giessen.de; Mark.Handy@geolo.uni-giessen.de)

(Received March 23, 1999; revised September 4, 1999; accepted October 19, 1999)